H. Hatzikirou, K. Böttger, A. Deutsch

Model-based Comparison of Cell Density-dependent Cell Migration Strategies

Erstveröffentlichung in / First published in:

Mathematical Modelling of Natural Phenomena. 2015, 10(1), S. 94-107 {Zugriff am: 13.03.2020}. Cambridge University Press. ISSN 1760-6101.

DOI: https://doi.org/10.1051/mmnp/201510105

Math. Model. Nat. Phenom.
Vol. 10, No. 1, 2015, pp. 94–107
DOI: 10.1051/mmnp/201510105

Model-based Comparison of Cell Density-dependent Cell Migration Strategies

H. Hatzikirou[1] *, K. Böttger[2], A. Deutsch[2]

[1] Center for Advancing Electronics Dresden, Technische Universität Dresden, 01062 Dresden, Germany

[2] Center for Information Services and High-Performance Computing, Technische Universität Dresden, 01062 Dresden, Germany

Abstract. Here, we investigate different cell density-dependent migration strategies. In particular, we consider strategies which differ in the precise regulation of transitions between resting and motile phenotypes. We develop a lattice-gas cellular automaton (LGCA) model for each migration strategy. Using a mean-field approximation we quantify the corresponding spreading dynamics at the cell population level. Our results allow for the prediction of cell population spreading based on experimentally accessible single cell migration parameters.

Keywords and phrases: cell migration strategies, non-linear diffusion, lattice-gas cellular automaton, mean-field approximation, spreading dynamics

Mathematics Subject Classification: 12A34, 56B78

1. Introduction

Cell migration is fundamental to tissue formation and regeneration, wound-healing as well as pathological processes such as cancer invasion. An important aspect of the afore-mentioned processes is the emergence of collectively moving cell populations. Different cell migration strategies allow for adaptation to microenvironmental conditions and influence the behavior of the moving cell population. In this manuscript, we compare the impact of different cell migration strategies on the cell population spreading dynamics.

A cell migration strategy can be viewed as the way a cell adapts its migration mode/phenotype to microenvironmental determinants. This corresponds to a special realization of phenotypic plasticity [10]. Cell migration modes have been originally classified based on the morphology of migration patterns. This terminology was then extended to include molecular parameters, such as cytoskeletal organization, the type of cell-matrix interaction and force generation, and the modification of the tissue structure imposed by migrating cells [7, 8, 12, 19].

In this article, we investigate two cell migration strategies which differ in the precise local cell density dependence. In particular, we consider strategies where increasing local cell density down-regulates or up-regulates cell motility. Our aim is to compare the impact of the two cell migration strategies on the population spreading dynamics. We develop a lattice-gas cellular automaton (LGCA) that has proven useful in the modelling and analysis of interacting and migrating cell populations [5, 11]. Upscaling

*Corresponding author. E-mail: haralambos.hatzikirou@tu-dresden.de

techniques such as mean-field approximations allow for the derivation of cell population level descriptions [3]. Here, we derive such macroscopic equations and calculate the time evolution of the mean square displacement (MSD) and cell density profiles to assess the spreading dynamics induced by each migration strategy. Then, we compare these approximations with corresponding LGCA simulations. Finally, we discuss the biological implications of our results.

2. Lattice-gas cellular automaton model

Our LGCA is defined on a two-dimensional square lattice $\mathcal{L} \subset \mathbb{Z}^2$. To every lattice node $\mathbf{r} \in \mathcal{L}$, velocity channels $(\mathbf{r}, \mathbf{c}_i)$, $i = 1, \ldots, b$, are associated. The parameter b defines the number of nearest neighbors on the lattice. Here, we choose $b = 4$ and $\mathbf{c}_i \in \{(1,0), (0,1), (-1,0), (0,-1)\}$. In addition, a fixed number of rest channels, $(\mathbf{r}, \mathbf{c}_i)$, $i = b+1, \ldots, K$, with $\mathbf{c}_i = \{(0,0)\}$ is introduced. The LGCA imposes an exclusion principle on channel occupation, i.e. at any time at most one cell is allowed in each channel at every lattice node. Thus K defines the maximal capacity of cells per node. We model explicitly two cell phenotypes, denoted by $\sigma \in \{m, r\}$: moving (m) and resting (r) cells. The occupation numbers at time k, $\eta_i(\mathbf{r}, k)$, $i = 1, \ldots, K$, are random Boolean variables that indicate the presence ($\eta_i = 1$) or absence ($\eta_i = 0$) of a cell in the channel $(\mathbf{r}, \mathbf{c}_i)$. The total number of cells at a node $\mathbf{r}$ and time k is defined by

$$n(\mathbf{r}, k) = n_m(\mathbf{r}, k) + n_r(\mathbf{r}, k) = \sum_{i=1}^{b} \eta_i(\mathbf{r}, k) + \sum_{i=b+1}^{K} \eta_i(\mathbf{r}, k),$$

where $n_m(\mathbf{r}, k)$ and $n_r(\mathbf{r}, k)$ are the number of moving and resting cells at a node $\mathbf{r}$ at time k, respectively.

2.1. LGCA dynamics

The dynamics of our LGCA arise from the repeated application of three operators: **propagation** ($\mathcal{P}$), **reorientation** ($\mathcal{O}$) and **switch** ($\mathcal{S}$).

The propagation and reorientation operators define cell movement, whereas the switch operator changes the phenotype of a cell. The composition $\mathcal{S} \circ \mathcal{O} \circ \mathcal{P}$ of the three operators is applied independently at every node $\mathbf{r}$ of the lattice and at each time k to evaluate the configuration at time $k + 1$, see Fig. 1. The precise update rules are described below. Since we assume that individual cells decide to switch independently from each other, the corresponding transition probabilities for the cell number per node follow a binomial distribution.

The phenotypic switching depends on the local cell density $\varrho = n/K \in [0, 1]$. Phenotypes are changed with probabilities $r_s(\varrho) \in [0, 1]$ and $1 - r_s(\varrho)$ that denote the probabilities of a moving cell to become resting and vice versa. We assume that the density dependence of the phenotypic switch is monotonous. Then, two strategies can be distinguished: **(S1) cell motility increases with local cell density** and **(S2) cell motility decreases with local cell density**.

Moreover, we will distinguish two kind of dependencies for each strategy: linear and non-linear with respect to local cell density $r_s(\varrho) \in [0, 1]$. The simplest phenotypic switch function is the linear density dependence:

$$r_s(\varrho) = A + B\varrho, \tag{2.1}$$

where $A, B \in \mathbb{R}$ with $(A + B) \in [0, 1]$. The non-linear switch involves a sigmoidal dependence on density, which has been already introduced in [2, 14, 18]:

$$r_s(\varrho) = \frac{\alpha_{min} + \alpha_{max}}{2} + \frac{\alpha_{max} - \alpha_{min}}{2} \tanh(\kappa(\varrho - \theta)), \tag{2.2}$$

where $\kappa \in \mathbb{R}$ denotes the steepness of the switch function and $\theta \in (0, 1)$ the critical cell density value at which the probabilities to switch from resting to moving and vice versa are equal. The parameters

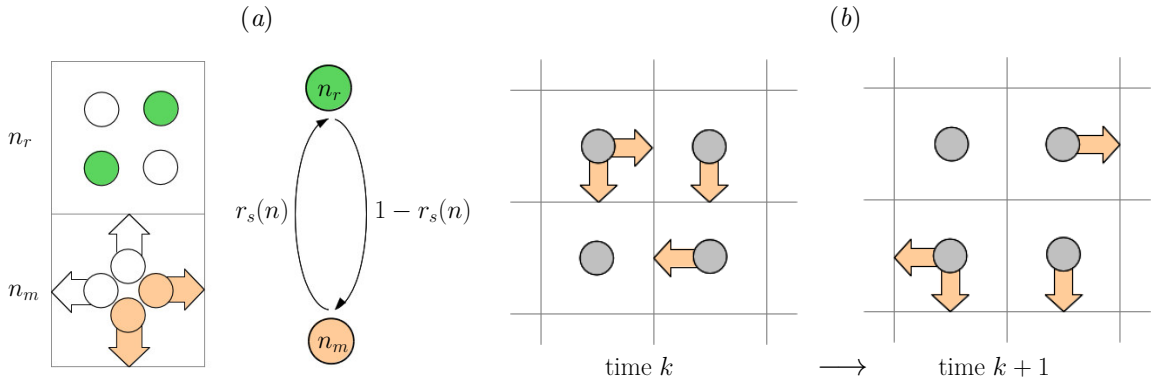

Figure 1. **LGCA dynamics:** CA model dynamics arise from repeated application of cell reactions (phenotypic switching) and cell migration. (1*a*) Left. Local state space at a given node is divided into rest channels and velocity channels. The cells in the rest channels, marked in green, are of resting phenotype. The cells in the velocity channels, marked in orange, have the migratory phenotype. White channels denote absence of cells. Right. Schematic illustration of model reactions. (1*b*) Example of cell propagation in the LGCA model. Cells in the velocity channels before and after a propagation step; orange arrows denote the presence of a cell in the respective velocity channel.

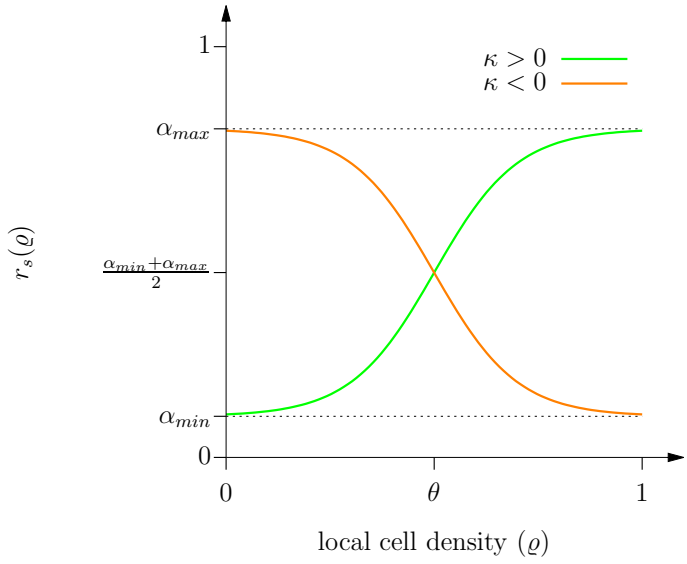

Figure 2. **Cell migration strategies:** Schematic illustration of the phenotypic switch function r_s which depends on the local cell density ϱ, see equation (2.2). The function r_s represents the probability that a cell is of resting phenotype and does not move. The parameter κ specifies the intensity of the switch density dependence. The case $\kappa > 0$ represents the (S2) strategy regulation and the $\kappa < 0$ is related to strategy (S1).

$\alpha_{min}, \alpha_{max} \in [0, 1]$, where $\alpha_{min} < \alpha_{max}$, denote the upper and lower bound of the switching probability. An illustration of (2.2) is shown in Figure 2.

In the LGCA simulation, we have implemented the following switching rules:

(1) Define $M_1 = \min(n_m, (K-b) - n_r)$ which is the potential number of cells that can switch from the moving to the resting phenotype, taking into account the effect of local volume exclusion. The transition probability that there are j_1 successful events "moving→resting" is modeled by

$$W^{\mathcal{S}}_{mr}((n_m, n_r)|(n_m - j_1, n_r + j_1)) = \begin{cases} \binom{M_1}{j_1} r_s(\varrho)^{j_1}(1 - r_s(\varrho))^{M_1 - j_1} & \text{if } 0 \le j_1 \le M_1, \\ 0 & \text{else.} \end{cases} \tag{2.3}$$

(2) Define $M_2 = \min(n_r, b - n_m)$ which is the potential number of cells that can switch from the moving to the resting phenotype, taking into account the effect of local volume exclusion. The transition probability that there are j_2 successful events "resting→moving" is given by

$$W^{\mathcal{S}}_{rm}((n_m, n_r)|(n_m + j_2, n_r - j_2)) = \begin{cases} \binom{M_2}{j_2} (1 - r_s(\varrho))^{j_2} r_s(\varrho)^{M_2 - j_2} & \text{if } 0 \le j_2 \le M_2, \\ 0 & \text{else.} \end{cases} \tag{2.4}$$

Finally, the difference between successful switches "moving→resting" and "resting→moving" is used to update the number of moving and resting cells so that $(n_m, n_r) \to (n_m - (j_1 - j_2), n_r + (j_1 - j_2)) = (n'_m, n'_r)$. Note that the switching process does not change the total number of cells but the ratio of moving and resting cells.

Subsequent to the switch operator, a reorientation step takes place where cells are randomly redistributed to the channels, providing a new local cell configuration at each node. In our model, only the cells of migratory phenotype move. Therefore, moving cells are distributed to the velocity channels, while resting cells are distributed to the resting channels, resulting in a configuration $\eta^{\mathcal{S}\circ\mathcal{O}}(\mathbf{r})$.

The final update step is the application of a propagation operator. Cells in the velocity channels, i.e. moving cells, are transported one lattice unit in directions determined by their velocities. The movement of cells in the propagation step is purely deterministic. The spatio-temporal automaton dynamics is therefore completely described by the mircodynamical equation

$$\eta_i(\mathbf{r} + \mathbf{c}_i, k+1) - \eta_i(\mathbf{r}, k) = \eta_i^{\mathcal{S}\circ\mathcal{O}}(\mathbf{r}, k) - \eta_i(\mathbf{r}, k) \in \{-1, 0, 1\},\ \mathbf{r} \in \mathcal{L},\ i = 1, \ldots, K,\ k = 0, 1, \ldots, \tag{2.5}$$

where the change in the occupation numbers is -1 if a channel looses a cell, 0 if nothing is changed and 1 if a channel gains a cell, respectively.

2.2. Scaling of the LGCA

We have chosen a non-dimensional scaling with unit lattice spacing and unit time scale $k \in \mathbb{N}$ in our LGCA simulation. Thus, cells residing at velocity channels move one lattice unit per unit time step. Our dimensionless simulations can easily be rescaled such that the temporal and spatial scales fit to specific applications. In our case, cell switching probabilities are related to the real dimensional mean time $T_m(\varrho)$ of a cell to stay in moving state and the mean time $T_r(\varrho)$ to stay in resting state, respectively, by

$$r_s(\varrho) = \frac{\tau}{T_m(\varrho)}, \quad 1 - r_s(\varrho) = \frac{\tau}{T_r(\varrho)}, \tag{2.6}$$

where τ is a sufficient small real dimensional time step length.

Besides scaling the LGCA time intervals, also the lattice spacing can be adjusted. If the lattice spacing is ϵ, the mean square displacement of a cell per time step τ in the LGCA is proportional to ϵ^2/τ. Thus, by scaling $\mathbf{x} = \epsilon\mathbf{r} \in \mathbb{R}$, the relationship between the LGCA motility and measured movement of cells is characterised by the diffusion constant $D = \epsilon^2/\tau$.

3. Jump process formulation and macroscopic dynamics

In order to analyse the cell population behavior, we derive a mean-field approximation for our LGCA model that can be analytically investigated. The main idea behind such an approach is to replace the description of interactions among many cells by a simplified description based on average (or effective) interactions. This reduces the multicellular nature of the problem into an effective formulation that can be stated in the form of macroscopic deterministic descriptions such as partial differential equations (PDE).

3.1. LGCA dynamics described by a jump process

Here, we adopt the convenient assumption that the LGCA dynamics describe a stochastic jump process which allows for the derivation of a single macroscopic equation. A jump process is a stochastic process that involves discrete spatial "jumps" at discrete times associated with the corresponding jump probabilities. Typically jump probabilities are stationary and depend on local information, such as local cell density.

3.1.1. Generalised master equation of a jump process

The general formulation of a jump process is given by the following master equation [13]:

$$P(\mathbf{r}, k+\tau) = \big[1 - \Phi(k)\big] P(\mathbf{r}, k) + \int_k^{k+\tau} \int_{\mathcal{L}} \phi(k+\tau-s) T(\mathbf{r}, \mathbf{r}') P(\mathbf{r}', s) d\mathbf{r}' ds, \tag{3.1}$$

where $T(\mathbf{r}, \mathbf{r}')$'s are the corresponding jump probabilities and $P(\mathbf{r}, k)$ the probability of finding a cell at node $\mathbf{r}$. The probability density function $\phi(k)$ corresponds to the waiting times of cells, i.e. the time that they need between two jumps, and $\Phi(k) = \int_k^{k+\tau} \phi(s) ds$ the probability of a cell staying at a specific node. As it is obvious, the waiting time distribution is related to the phenotypic switch dynamics, since the operator $\mathcal{S}$ dictates the onset of cells' motility.

The jump probabilities correspond to the random walk dynamics of our LGCA, i.e. it is equiprobable to jump from node $\mathbf{r}$ to an adjacent node $\mathbf{r} + \mathbf{c}_i$. Then the jump probabilities read as:

$$T(\mathbf{r}, \mathbf{r} + \mathbf{c}_i) = \frac{1}{b} \sum_{i=1}^{b} \delta(\mathbf{r}, \mathbf{r} + \mathbf{c}_i), \tag{3.2}$$

where the delta of Kronecker is $\delta(x, y) = 1$ if $x = y$, else $\delta(x, y) = 0$.

As stated above, the phenotypic switch is associated with the waiting time distribution. The operator $\mathcal{S}$ implies a Markov chain with transition probabilities (2.3) and (2.4). Therefore, the waiting times of changing an automaton state (n_r, n_m) are exponentially distributed with probability distribution function $\phi(k) = \lambda e^{-\lambda k}$ and the corresponding cumulative distribution is $\Phi(k) = \int_k^{k+\tau} \phi(k+\tau-s) ds = 1 - \lambda$. Therefore, the problem is reduced to calculate the rate λ that denotes the rate of a resting cell becoming motile related to the transition probability $W_{rm}^{\mathcal{S}}$ (2.4).

3.1.2. Calculation of jump waiting time λ

The dynamics of the switch operator can be described by the following master equation

$$\frac{d}{dt} P^{\mathcal{S}}(n_r, n_m) = \mathbf{W}^{\mathcal{S}} P^{\mathcal{S}}(n_r, n_m), \tag{3.3}$$

where $P^{\mathcal{S}}(n_r, n_m)(\mathbf{r}, k)$ is the probability of finding n_r resting cells and n_m moving cells at a node $\mathbf{r}$ at time k, within the context of the switch operator $\mathcal{S}$ for a time step $[k, k+\tau)$, and $\mathbf{W}^{\mathcal{S}}$ the corresponding transition probability matrix. For simplicity the spatiotemporal arguments have been omitted. During the application of operator $\mathcal{S}$ the number of total cells within the node is constant. Then applying the

formula $P^{\mathcal{S}}(n = n_r + n_m) = \sum_{n_r} P^{\mathcal{S}}(n_r, n - n_r) = \sum_{n_m} P^{\mathcal{S}}(n - n_m, n_m)$ to the switch operator master equation (3.3):

$$\sum_{n_r} \frac{d}{dt} P^{\mathcal{S}}(n_r, n - n_r) = \frac{d}{dt} P^{\mathcal{S}}(n) = 0,$$

since the operator is mass conserving. The above equation implies that:

$$\sum_{n_r} \mathbf{W}^{\mathcal{S}} P^{\mathcal{S}}(n_r, n - n_r) = \sum_{n_m} \mathbf{W}^{\mathcal{S}} P^{\mathcal{S}}(n - n_m, n_m), \tag{3.4}$$

From the left hand side of the (3.4), we can easily calculate the average flux of cells from resting to moving J^S_{rm}:

$$\begin{aligned} J^S_{rm} &= \sum_{n_r} \sum_{z} W^{\mathcal{S}}_{rm}\big((n_m, n_r)|(n_r - z, n_m + z)\big) P^{\mathcal{S}}(n_r - z, n_m + z) \\ &= \sum_{n_r} \sum_{z} W^{\mathcal{S}}_{rm}\big((n_r + z, n_m - z)|(n_r, n_m)\big) P^{\mathcal{S}}(n_r, n_m) \\ &= \sum_{n_r} \sum_{z} z \binom{M_2}{z} \big(1 - r_s(\varrho)\big)^z r_s(\varrho)^{M_2 - z} P^{\mathcal{S}}(n_r, n - n_r) \\ &= \big(1 - r_s(\varrho)\big) \sum_{n_r} M_2 P(n_r, n - n_r). \end{aligned} \tag{3.5}$$

The above relation involves node capacity restriction effects due to the presence of $M_2 = \min(n_r, b - n_m)$, see equation (2.4). By assuming a low density regime $\varrho \ll 1$, it is $M_2 = n_r$. Therefore, for constant n the above equation yields

$$J^S_{rm} = \big(1 - r_s(\varrho)\big)\langle n_r \rangle,$$

where $\langle \cdot \rangle$ denotes an ensemble average. Similarly, we can elaborate the right hand side of equation (3.5) and find out that equals to $J^S_{mr} = r_s(\varrho)\langle n - n_r \rangle$. From the equilibrium condition $J^S_{mr} = J^S_{rm}$ we obtain:

$$\begin{aligned} \langle n_r \rangle \big(1 - r_s(\varrho)\big) &= \langle n - n_r \rangle r_s(\varrho) \\ \langle n_r \rangle &= r_s(\varrho)\langle n \rangle. \end{aligned} \tag{3.6}$$

Thus, at the mean-field limit of the process, the fluxes of moving and resting cells are $J^S_{rm} = (1 - r_s(\varrho)) r_s(\varrho)\langle n \rangle = J^S_{mr}$. Please note, the switch dynamics are equilibrated only for their average behavior, whereas the whole probability distribution $P^{\mathcal{S}}(n_r, n_m)$ is not necessary at steady state.

From the above discussion, we can easily conclude that the average jump rate is

$$\lambda = J^S_{rm} / \langle n_r \rangle = 1 - r_s(\varrho),$$

which is inversely proportional to the average time of a cell staying at a resting state $T_r(\varrho)$, see (2.6). Please note, the latter is only possible in the context of low density assumption, since for high densities capacity effects should be included. After the calculation of the parameter λ, we are now able to explicitly formulate the jump process master equation:

$$P(\mathbf{r}, k + 1) = r_s(\varrho(\mathbf{r}, k)) P(\mathbf{r}, k) + \sum_{i=1}^{b} \frac{1 - r_s(\varrho(\mathbf{r} + \mathbf{c}_i, k))}{b} P(\mathbf{r} + \mathbf{c}_i, k). \tag{3.7}$$

3.2. Mean-field approximation of low density LGCA dynamics

In this Section, we are interested in the average behavior of the system. Therefore, we can average the jump process master equation (3.7) by applying to both sides the operation $\sum_n n$, since the local cell

density is defined as $\rho(\mathbf{r},k)=\langle\varrho(\mathbf{r},k)\rangle=K^{-1}\sum_n nP(\mathbf{r},k)$, and obtain:

$$\rho(\mathbf{r},k+1)=\langle r_s(\varrho(\mathbf{r},k))\rangle\rho(\mathbf{r},k)+\sum_{i=1}^{b}\frac{1-\langle r_s(\varrho(\mathbf{r},k))\rangle}{b}\rho(\mathbf{r}+\mathbf{c}_i,k). \tag{3.8}$$

Due do the mean-field assumption, we obtain $\langle r_s(\varrho(\mathbf{r},k))\rangle\approx r_s(\rho(\mathbf{r},k))$. In combination with the low density assumption (see previous Section), we approximate $r_s(\rho)$ for small cell densities as $r_s(\rho)=r_s(0)+r_s'(0)\rho+\mathcal{O}(\rho^2)=A+B\rho+\mathcal{O}(\rho^2)$ and equation (3.8) becomes

$$\rho(\mathbf{r},k+1)=A\rho(\mathbf{r},k)+B\rho^2(\mathbf{r},k)+\frac{1}{b}\sum_{i=1}^{b}(1-A)\rho(\mathbf{r}+\mathbf{c}_i,k)-B\rho^2(\mathbf{r}+\mathbf{c}_i,k). \tag{3.9}$$

To convert (3.9) into a continuous macroscopic PDE, we identify the average density $\rho(\mathbf{r},k)$ by its continuous counterpart $\rho(\mathbf{x},t)$, where $\mathbf{x}=\mathbf{r}\epsilon\in\mathbb{R}$ and $t=k\tau\in\mathbb{R}_+$, with $\epsilon,\tau\in\mathbb{R}_+$, which gives

$$\rho(\mathbf{x},t+1)=A\rho(\mathbf{x},t)+B\rho^2(\mathbf{x},t)+\frac{1}{b}\sum_{i=1}^{b}(1-A)\rho(\mathbf{x}+\epsilon\mathbf{c}_i,t)-B\rho^2(\mathbf{x}+\epsilon\mathbf{c}_i,t). \tag{3.10}$$

Expanding all terms in (3.10) in a truncated Taylor series in powers of ϵ and τ up to second order gives

$$\rho+\tau\partial_t\rho+\frac{\tau^2}{2}\partial_{tt}\rho=A\rho+B\rho^2+\frac{1-A}{b}\sum_{i=1}^{b}\left(\rho+\epsilon J(\mathbf{x})\mathbf{c}_i+\frac{\epsilon^2}{2}\mathbf{c}_i^TH(\mathbf{x})\mathbf{c}_i\right) \tag{3.11}$$

$$-\frac{B}{b}\sum_{i=1}^{b}\left(\rho^2+2\epsilon\rho J(\mathbf{x})\mathbf{c}_i+\epsilon^2(J(\mathbf{x})\mathbf{c}_i)^TJ(\mathbf{x})\mathbf{c}_i+\epsilon^2\rho\mathbf{c}_i^TH(\mathbf{x})\mathbf{c}_i\right)$$

where J is the Jacobian matrix and H the Hessian matrix. For the sake of clarity, we have droped the temporal t and the spatial argument $\mathbf{x}$. To proceed, we consider the diffusive limit, i.e. $\epsilon\to0$, $\tau\to0$ and $\lim_{\epsilon,\tau\to0}\frac{\epsilon^2}{\tau}=const:=D$. This gives

$$\partial_t\rho=\frac{1-A}{b}\frac{D}{2}\sum_{i=1}^{b}\mathbf{c}_i^TH(\mathbf{x})\mathbf{c}_i-\frac{B}{b}D\sum_{i=1}^{b}(J(\mathbf{x})\mathbf{c}_i)^TJ(\mathbf{x})\mathbf{c}_i-\frac{B}{b}D\rho\sum_{i=1}^{b}\mathbf{c}_i^TH(\mathbf{x})\mathbf{c}_i. \tag{3.12}$$

Taking into account the channel's symmetry it is

$$\partial_t\rho=\frac{1-A}{b}D\nabla^2\rho-BD(\nabla\rho)^2-BD\rho\nabla^2\rho=\underbrace{D\left(\frac{1-A}{2}-B\rho\right)}_{=:\mathcal{D}(\rho)}\nabla^2\rho+D\underbrace{(-B)}_{=\mathcal{D}'(\rho)}(\nabla\rho)^2 \tag{3.13}$$

Finally, the jump process of our LGCA can be approximated by a degenerate diffusion equation

$$\partial_t\rho=D\nabla(\mathcal{D}(\rho)\nabla\rho)\ . \tag{3.14}$$

The resulting non-linear diffusion coefficient $\mathcal{D}(\rho)=\frac{1-A}{2}-B\rho$ fulfils our intuition since (i) if $B=0$ then we expect a constant coefficient, and (ii) for $A=0$ the expected diffusion coefficient in one dimension is $1/2$. Moreover, for $A>0$ and $B=0$ the $r_s(\rho)=A>0$ indicates a tendency of cells to rest and therefore implies a reduced diffusion coefficient $(1-A)/2<1/2$. In the following, we test the validity of our PDEs and we showcase their resulting behavior.

3.3. Comparison of the PDE approximation and the LGCA dynamics

In this Section, we compare the derived PDE approximation (3.14) with the LGCA simulations. Let us consider a square lattice $(r_x, r_y) \in \mathcal{L} = L_x \times L_y$ with periodic boundary condition on the L_y-axis, that is $n(r_x, r_y = 0, k) = n(r_x, r_y = L_y, k)$ for all $r_x \in [0, L_x]$, $k \in \mathbb{N}$, and open boundary conditions on the L_x-axis. The initial condition of the simulations is a thin stripe of cells located along the center line column $r_x = \frac{L_x}{2}$. A typical simulation lasts for 1000 time steps. In order to study cell motility, we reduce the two-dimensional system to one dimension by averaging the concentration profile along the L_y-axis that is $\tilde{\varrho}(r_x, k) := \frac{1}{|L_y|}\sum_{r_y \in |L_y|} \varrho(k)$. The observable that characterizes the motility rate of cells is the mean square displacement (MSD)

$$\langle r_x^2(k)\rangle = \sum_{r_x \in L_x} \left(r_x - \frac{L_x}{2}\right)^2 \tilde{\varrho}(r_x, k).$$

The above simulation set up reduces the problem of calculating the MSD to one dimension (please see Appendix). Then, by means of our resulting mean-field approximation (3.14), we can calculate the corresponding time evolution of MSD in one dimension as:

$$\frac{d}{dt}\langle x^2(t)\rangle = \int_{\mathbb{R}} x^2 \partial_t \rho dx = D \int_{\mathbb{R}} x^2 \partial_x(\mathcal{D}(\rho)\partial_x \rho)\ dx. \tag{3.15}$$

Using integration by parts and assuming appropriate boundary conditions, i.e. $\partial_t \rho(x,t)\Big|_{\pm\infty} = \rho(x,t)\Big|_{\pm\infty} = 0, \forall t \in \mathbb{R}_+$, we finally obtain for phenotypic switches in the form of $r_s(\rho) = A + B\rho$ the following equation:

$$\frac{d}{dt}\langle x^2(t)\rangle = D'(0)\int_{\mathbb{R}} \rho^2(x,t)dx + D(0)\int_{\mathbb{R}} \rho(x,t)dx, \tag{3.16}$$

with $D(0) = D(1-A) = 2D\mathcal{D}(0)$, $D'(0) = D\mathcal{D}'(0) = -DB$. It is evident in the absence of density dependence in the phenotypic switch function, $B = 0$, the MSD reduces to the classical relationship:

$$\langle x^2(t)\rangle = D(0)t, \tag{3.17}$$

for initial conditions $\langle x^2(0)\rangle = 0$ and for normalised cell density $\int_{\mathbb{R}} \rho(x,t)dx = 1$. However, the existence of density dependence can potentially change the MSD time evolution since the integral term in equation (3.16) may converge to zero for growing time or stay persistently different than zero. Since analytical treatment of the one dimensional equation (3.16) is non-trivial, we solve it numerically[1]. In particular, we use periodic boundary conditions in the y-axis combined with a sufficiently large domain to avoid boundary effects and define an initial cell density corresponding to the initial condition used in the LGCA.

We simulate the LGCA and approximated PDE model for two selected examples, the linear phenotypic switch function (2.1) and the sigmoidal shaped switch function (2.2). According to the mean-field derivation, our PDE approximation is only valid for small cell densities values in order to avoid node capacity effects. From equation (3.9), we can easily observe that the term $B\rho^2(\mathbf{x}, t)$ for large B introduces errors in the corresponding mean-field approximation, since we have assumed that the local fluctuations are zero, i.e. $\langle \varrho^2(\mathbf{x}, t)\rangle \approx \langle \varrho(\mathbf{x}, t)\rangle^2 = \rho^2(\mathbf{x}, t)$. Therefore, we expect for $B \ll 1$ a good agreement of equation (3.14) solution with the actual LGCA dynamics for long enough times. In particular, for early simulation times, when all cells are around a point, the deviation between LGCA and the corresponding PDE is enhanced. In the long run, cell spreading improves the performance of our mean-field approximation, since $\rho(\mathbf{x}, t) \to 0$. Moreover, B increases the impact of the integral term in equation (3.16), that is more

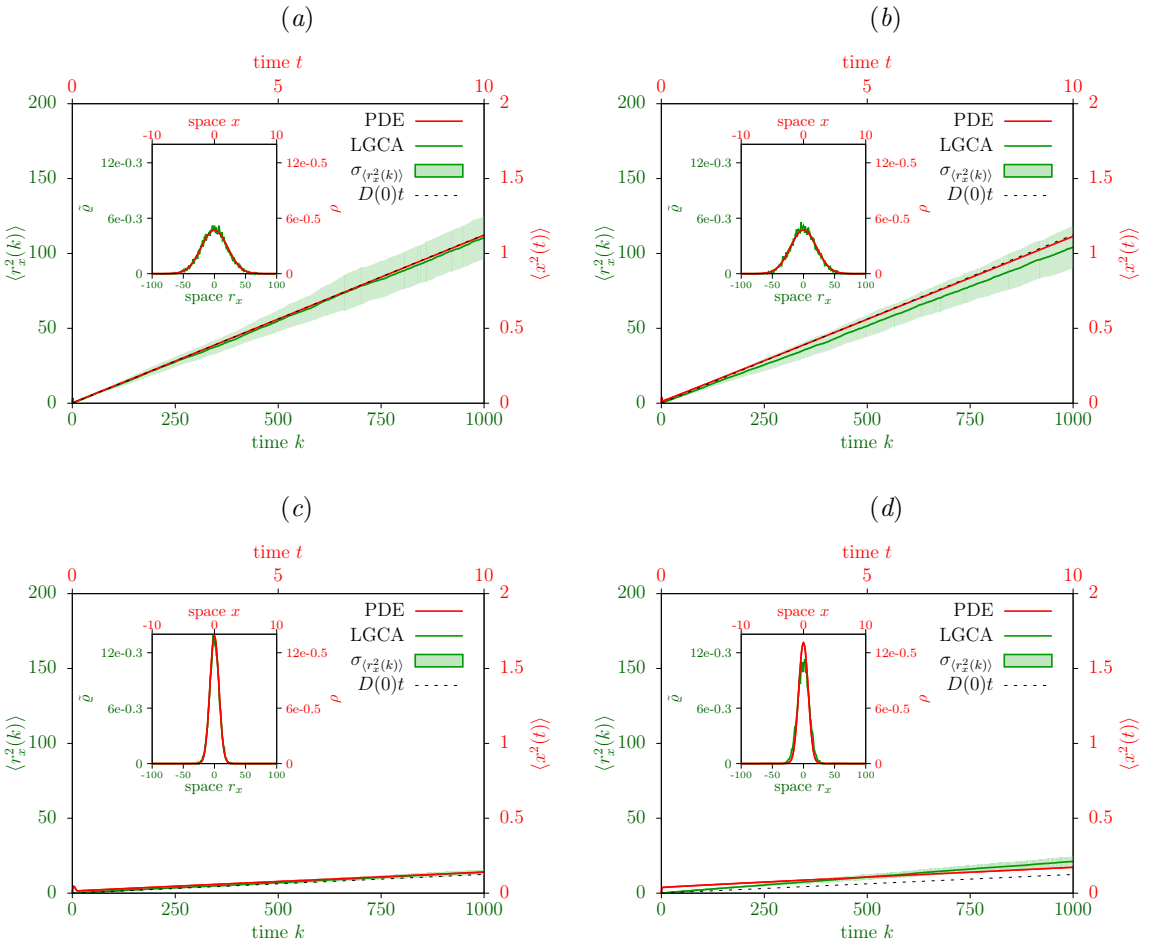

Figure 3. **Comparison of PDE approximation and LGCA simulation for linear phenotypic switch function:** The phenotypic switch function is given by $r_s(\rho) = A + B\rho$. Figure (3*a*) and (3*b*) correspond to strategy (S1) with phenotypic switch parameters $A = 0.1$, $B = 0.1$ and $A = 0.1$, $B = 0.5$, respectively. Figure (3*c*) and (3*d*) correspond to strategy (S2) with phenotypic switch parameters $A = 0.9$, $B = -0.1$, and $A = 0.9$, $B = -0.5$, respectively. LGCA simulations are performed for 1000 iteration steps and average over 100 simulation runs. The PDE is scaled by $\epsilon = 10^{-1}$ resulting into $(\mathbf{x}, t) = (10^{-1}\mathbf{r}, 10^{-2}k)$ and with diffusion coefficient $D = 1$. The initial cell density is given by $\tilde{\varrho}(r_x, 0) = \rho(x, 0) = 0.25$ for $r_x = x = 0$. Each Figure shows the comparison of the time evolution of the mean square displacement and the cell density profile of the LGCA and the PDE after 1000 iteration steps (inlet).

prominent in early times of the simulation. However, we are more interested in the long-term behavior of the MSD.

For the case where the phenotypic switch depends linearly on local density and for $B \ll 1$ the mean-field MSD $\langle x^2(t)\rangle$ agrees well with the one calculated directly from LGCA simulations $\langle r_x^2(k)\rangle$ (see Figure 3(*a*) and 3(*c*)). In particular, due to the fast spreading the integral term of equation (3.16) becomes insignificant and the MSD is dominated by the linear term $D(0)t$. For the linearly increasing switch

[1]We solve the degenerate diffusion equation (3.14) numerically in one dimension using the open source package XMDS (code available from http://www.xmds.org) [4].

($B > 0$) increasing B implies a deviation of the two MSD estimations mainly due to the impact of local fluctuations (Figure 3(b)). In particular, due to the fast spreading the integral term of equation (3.16) becomes insignificant and the MSD is dominated by the linear term $D(0)t$. On the other hand, in the linearly decreasing phenotypic switch ($B < 0$), large B introduces errors to the analytic approximation when compared to the automaton MSD. Moreover, the time evolution of the analytic MSD is initially strongly non-linear since the impact of the integral term in equation (3.16) is dominant (Figure 3(d)).

For the case where the phenotypic switch sigmoidally depends on local density, a low-density linearised version $r_s(\rho) = r_s(0) + r_s'(0)\rho + \mathcal{O}(\rho^2)$ is used for the continuous estimation of MSD (3.16). Of course, the corresponding automaton MSD calculation involves the full sigmoidal switch function. The resulting continuous MSD strongly relies on the value of

$$B = r_s'(0) = \frac{\alpha_{max} - \alpha_{min}}{2}\kappa\big[1 - \tanh^2(-\kappa\theta)\big],$$

which obviously depends on the value of the parameters κ and θ. In our examples, we have used $\kappa = \pm 8$ which implies steep sigmoidal switches and significantly differs from the linear switch. Again for $B \ll 1$, e.g. for the high θ value, we observe again an excellent agreement of the MSDs calculated from the LGCA and the corresponding PDE (see Figure 4(a) and 4(c)). As stated before, for large B we observe again a small deviation of the analytically calculated MSDs with the corresponding LGCA ones. Interestingly, for very small θ the integral term becomes dominating and the sign of B, that follows the sign of κ, introduces a negative correlation of the linear contribution $\mathcal{D}(0)t$ with the full MSD evolution (see Figure 4(b), 4(d)).

4. Discussion

In this article, we developed a lattice-gas cellular automaton model to compare density-dependent cell migration strategies. In the model, we distinguish two cell phenotypes, migratory and resting, and we assume that cells change their phenotype depending on the local cell density. We study two opposing strategies, (S1) cell motility increases with local cell density and (S2) cell motility decreases with local cell density. In addition, we assume for both strategies linear and sigmoidal dependencies on the local cell density. The model facilitates the derivation of a macroscopic cell population description. We derive analytic formulations for the two migration strategies which correspond to non-linear degenerate diffusion equations. Subsequently, we compare the time evolution of the population spreading behavior for the two migration strategies. Finally, we show that the mean-field PDE is a good approximation for specific parameter regimes when compared to LGCA simulations with respect to the resulting mean square displacement.

Our mathematical model considers local cell density as mediator of cell migration regulation. Cell density is known to be correlated with nutrient gradients, secreted factors, as well as oxygen or toxic metabolites [9,10,17,20]. The dependence of cell migration on local cell density implies adaptation to the current microenvironmental conditions, here mediated by the cell density. So far only a few experimental studies have attempted to quantify the role of cell density as a cell migration regulator, e.g. [15]. We believe that a more precise quantification of cell density effects on migration is crucial for a better distinction of cellular and non-cellular influences on the precise regulation of cell migration strategies.

Our model allows to study the impact of micro-environmental heterogeneity. The probabilistic switch between moving and resting phenotypes indirectly models other micro-environmental factors than local cell density that impact cell motility. In particular, the limit values of the phenotypic switch function can be associated with the uncertainty in a cell's decision, over a resting or a motile state, for the different local density values. In other words, if $\min_\rho\{r_s(\rho)\} = 0$ and $\max_\rho\{r_s(\rho)\} = 1$ then the cell deterministically decides to move or to rest according to local cell density. However, relaxing these limiting values a "noise" in the cell motility regulation is introduced, interpreted as the effective impact of other micro-environmental factors, such as extracellular matrix components. Finally, a spatial distribution of these limiting values of the switching function may account for a measure of micro-environmental heterogeneity

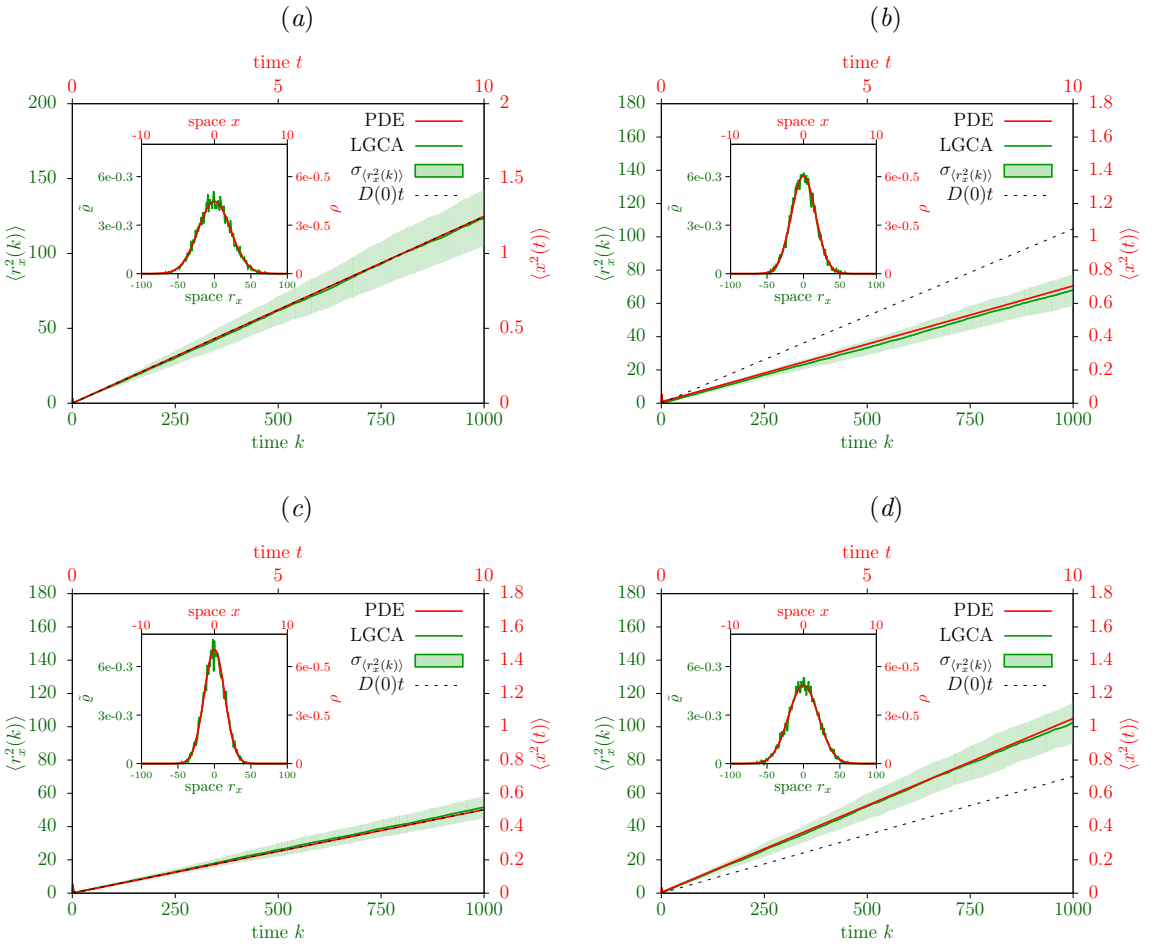

Figure 4. **Comparison of PDE approximation and LGCA simulation for sigmoidal phenotypic switch function:** The phenotypic switch function is given by $r_s(\varrho) = \frac{\alpha_{min}+\alpha_{max}}{2} + \frac{\alpha_{max}-\alpha_{min}}{2}\tanh(\kappa(\varrho-\theta))$. Parameters are $\alpha_{min} = 0$, $\alpha_{max} = 0.6$, $K = 8$. Figure $(4a)$ and $(4b)$ correspond to strategy (S1) with , $\theta = \frac{3}{8}$, $\kappa = 8$ and $\theta = \frac{1}{16}$, $\kappa = 8$, respectively. Figure $(4c)$ and $(4d)$ correspond to strategy (S2) with , $\theta = \frac{3}{8}$, $\kappa = -8$ and $\theta = \frac{1}{16}$, $\kappa = -8$, respectively. LGCA simulations are performed for 1000 iteration steps and average over 100 simulation runs.The PDE is scaled by $\epsilon = 10^{-1}$ resulting into $(\mathbf{x}, t) = (10^{-1}\mathbf{r}, 10^{-2}k)$ and with diffusion coefficient $D = 1$. The initial cell density is given by $\tilde{\varrho}(r_x, 0) = \rho(x, 0) = 0.25$ for $r_x = x = 0$. Each Figure shows the comparison of the time evoultion of the mean square displacement and the cell density profile of the LGCA and the PDE after 1000 iteration steps (inlet).

impacting cell migration regulation. In the future, we are planning to precisely quantify heterogeneity with respect to different micro-environmental parameters.

One possible biological application of our model may be the investigation of the transition between mesenchymal and epithelial cells [1, 19]. The mesenchymal migration mode is characterised by high cell motility, proteolytic degradation of extracellular matrix, lack of cell polarity and down-regulation of cell-cell adhesion. On the other hand, epithelial cells are immotile, connected by strong adhesion bonds and exhibit regular shapes. Epithelial and mesenchymal phenotypes can be interpreted as two migration modes, resting and motile, respectively. In recent experimental studies [15], it has been demonstrated

that in the case of MET increasing local cell density mediates the inhibition of cell migration. On the other hand, there is experimental evidence that relates the epithelial-mesenchymal transition (EMT) to cell density modulations [6,16]. Translated into our model, the mesenchymal-epithelial transition (MET) corresponds to strategy (S1), whereas the epithelial-mesenchymal transition (EMT) could be related to strategy (S2). However, further research is required to establish this association, since we lack enough biological evidences specially for the EMT case.

A. Equivalence of 2D cylindric and 1D cartesian diffusion equation.

It is important to show that the simulation setting, described in Section 3, reduces the dimension of the system but it does not influence the qualitative behavior of the LGCA. In the following, we show that the diffusion coefficient is identical both in free boundary 2D simulations and in simulations with periodic B.C. on the L_y-axis.

The evolution of a system on a lattice with periodic B.C. on the L_y-axis can be seen as an evolution on a cylindrical surface with open B.C., resembling the "evolution on a tube". Therefore, the macroscopic dynamics of the system can be realized by the diffusion equation in cylindrical coordinates. In particular, a classical diffusion equation in cylindrical coordinates $(x, y, z) = (r\cos\theta, r\sin\theta, z)$ yields

$$\frac{\partial}{\partial t}\rho(r,\theta,z,t) = D\Big[\frac{1}{r}\frac{\partial}{\partial r}\big(r\frac{\partial}{\partial r}\big) + \frac{1}{r^2}\frac{\partial^2}{\partial\theta^2} + \frac{\partial^2}{\partial z^2}\Big]\rho(r,\theta,z,t), \tag{4.1}$$

with boundary conditions $\rho(r,\theta = 0,z,t) = \rho(r,\theta = 2\pi,z,t)$ and $\partial_\theta\rho(0) = \partial_\theta\rho(2\pi)$. Moreover, the variable radial coordinate is fixed as $r = r_0 = |L_y|/2\pi$. Thus, eq. (5.1) simplifies to

$$\rho_t = D\rho_{zz} + \frac{4\pi^2 D}{|L_y|^2}\rho_{\theta\theta}, \tag{4.2}$$

In order to reduce the system dimension to 1D, we integrate along the angular coordinate θ and the quantity of interest is the normalized averaged cell density along the L_y-axis

$$\tilde{\rho} = \frac{1}{2\pi}\int_0^{2\pi}\rho\frac{|L_y|}{2\pi}d\theta.$$

We derive the evolution equation for $\tilde{\rho}$ by integrating eq. (5.2) over θ, previously multiplied by $|L_2|/4\pi^2$

$$\tilde{\rho}_t = D\tilde{\rho}_{zz} + \frac{2\pi D}{|L_y|^2}\int_0^{2\pi}\rho_{\theta\theta}\frac{|L_y|}{2\pi}d\theta = D\tilde{\rho}_{zz} + \frac{D}{|L_y|}\big[\rho_\theta(2\pi) - \rho_\theta(0)\big]. \tag{4.3}$$

The last term is obviously zero due to the periodic B.C. of the system. Thus, we obtain the equation

$$\tilde{\rho}_t = D\tilde{\rho}_{zz}. \tag{4.4}$$

The above equation shows that the "tube" simulation setup and the dimension reduction process (through averaging along the L_y-axis) to the L_x-axis does not change the diffusion coefficient of the original system. Thus, the mean square displacement will remain intact, i.e. $\langle z^2\rangle = 2Dt$.

Acknowledgements. HH acknowledges the support of the German Research Foundation (DFG) within the Cluster of Excellence "Center for Advancing Electronics Dresden" (EXC1056) and the support of BMBF for the eMED project SYSIMIT (01ZX1308D).

References

[1] C. L. Chaffer, E. W. Thompson, E. D. Williams. *Mesenchymal to epithelial transition in development and disease.* Cells Tissues Organs, 185 (2007), 7–19.

[2] A. Chauvière, L. Preziosi, H. Byrne *A model of cell migration within the extracellular matrix based on a phenotypic switching mechanism.* Math. Med. Biol., 27 (2010), 255–81.

[3] B. Chopard, M. Droz. *Cellular automata modeling of physical systems.* Cambridge University Press (1998).

[4] G. R. Dennis, J. J. Hope, M. T. Johnsson. *XMDS2: Fast, scalable simulation of coupled stochastic partial differential equations.* Comput. Phys. Commun., 184 (2013), 201–208.

[5] A. Deutsch, S. Dormann. *Cellular automaton modeling of biological pattern formation.* Birkhäuser (2005).

[6] K. Doxzen, S. R. Vedula, M. C. Leong, H. Hirata, N.S. Gov, A. J. Kabla, B. Ladoux, C.T. Lim. *Guidance of collective cell migration by substrate geometry.* Integr. Biol. (Camb.), 5 (2013), 1026–35.

[7] P. Friedl, K.ZS. Zänker, E.B. Bröcker. *Cell migration strategies in 3-D extracellular matrix: differences in morphology, cell matrix interactions, and integrin function.* Microsc. Res. Tech., 43 (1998), 369–78.

[8] P. Friedl. *Prespecification and plasticity: shifting mechanisms of cell migration.* Curr. Opin. Cell Biol., 16 (2004), 14–23.

[9] E. Favaro, G. Nardo, L. Persano, M. Masiero, L. Moserle, R. Zamarchi, E. Rossi, G. Esposito, M. Plebani, U. Sattler et al. *Hypoxia inducible factor-1alpha inactivation unveils a link between tumor cell metabolism and hypoxia-induced cell death.* Am. J. Pathol., 173 (2008), 1186–201.

[10] P. Friedl, D. Gilmour. *Collective cell migration in morphogenesis, regeneration and cancer.* Nat. Rev. Mol. Cell. Biol., 10 (2009), 445–57.

[11] H. Hatzikirou, D. Basanta, M. Simon, C. Schaller, A. Deutsch. *'Go or Grow': the key to the emergence of invasion in tumor progression?* Math. Med. Biol., 29 (2012), 49–65.

[12] T. Lämmermann, M. Sixt. *Mechanical modes of 'amoeboid' cell migration.* Curr. Opin. Cell Biol., 21 (2009), 636-644.

[13] H. Othmer, S. Dunbar, W. Alt. *Models of dispersal in biological systems.* J. Math. Biol., 26 (1988), 263-98.

[14] K. Pham, A. Chauvière,H. Hatzikirou, X. Li, H. Byrne, V. Cristini, J. Lowengrub. *Density-dependent quiescence in glioma invasion: instability in a simple reaction-diffusion model for the migration/proliferation dichotomy.* J. Biol. Dyn., 6 (2012), 54–71.

[15] A. Puliafito, L. Hufnagela, P. Neveua, S. Streichan, A. Sigal, D. Kuchnir Fygenson, and B. I. Shraiman. *Collective and single cell behavior in epithelial contact inhibition.* Proc. Natl. Acad. Sci. U.S.A., 109 (2012), 739–44.

[16] D. Sarrio, S. M. Rodriguez-Pinilla, D. Hardisson, A. Cano, G. Moreno-Bueno, J. Palacios. *Epithelial-mesenchymal transition in breast cancer relates to the basal-like phenotype.* Cancer Res., 68 (2008), 989–97.

[17] S. L. Schor, A. M. Schor. *Foetal-to-adult transitions in fibroblast phenotype: their possible relevance to the pathogenesis of cancer.* J. Cell Sci. Suppl., 8 (1987), 165–80.

[18] M. Tektonidis, H. Hatzikirou, A. Chauvière, M. Simmon, K. Schaller, A. Deutsch. *Identification of intrinsic in vitro cellular mechanisms for glioma invasion.* J. Theor. Biol., 21 (2011), 131–47.

[19] J. P. Thiery. *Epithelial-mesenchymal transitions in tumour progression.* Nat. Rev. Cancer, 2 (2002), 442–454.

[20] A. Vultur, J. Cao, R. Arulanandam, J. Turkson, R. Jove, P. Greer, A. Craig, B. Elliott, L. Raptis. *Cell-to-cell adhesion modulates Stat3 activity in normal and breast carcinoma cells.* Oncogene, 23 (2004), 2600–16.

Table 1. List of symbols

LGCA notation	
$\mathcal{L} \subset \mathbb{Z}^d$	d-dimensional regular square lattice
$\mathbf{r} \in \mathcal{L}$	node on the lattice
$\sigma \in \{m, r\}$	cell type in the model (moving m and resting r)
$K \geq 2d$	capacity of each lattice node ($2d$ velocity channels and $K-2d$ resting channels)
$n(\mathbf{r}, k) \in \{0, \ldots, K\}$	cell number at a node $\mathbf{r}$ and time k
$\varrho(\mathbf{r}, k) = n(\mathbf{r}, k)/K$	cell density at a node $\mathbf{r}$ and time k ($0 \leq \varrho(\mathbf{r}, k) \leq 1$)
$\rho(\mathbf{r}, k) = \langle n(\mathbf{r}, k) \rangle / K$	mean cell density at a node $\mathbf{r}$ and time k ($0 \leq \rho(\mathbf{r}, k) \leq 1$)
$k \in \mathbb{N}$	automaton time step
r_s	probability that a moving cell changes to resting
$1 - r_s$	probability that a resting cell changes to moving
$\kappa \in \mathbb{R}$	intensity of the phenotypic switch
$\theta \in (0, 1)$	critical cell density value at which the probabilities to switch from resting to moving and vice versa are equal
$\mathrm{P}(\cdot)$	probability
T_m	mean time of a cell to stay in moving state
T_r	mean time of a cell to stay in resting state